

Hydroxyapatite/Mesoporous Graphene/Single-Walled Carbon Nanotubes Freestanding Flexible Hybrid Membranes for Regenerative Medicine

Rujing Zhang, Noah Metoki, Orna Sharabani-Yosef, Hongwei Zhu,* and Noam Eliaz*

Freestanding flexible membranes based on biocompatible calcium phosphates are of great interest in regenerative medicine. Here, the authors report the first synthesis of well-aligned biomimetic hexagonal bars of hydroxyapatite (HAp) on flexible, freestanding mesoporous graphene/single-walled carbon nanotubes (MG/SWCNT) hybrid membranes. The chemical composition and surface morphology of the HAp coating resemble those of biological apatite. Nitrogen doping and oxygen plasma etching of the MG/SWCNT membranes increase the density of nucleation sites and yield more uniform coatings. This novel membrane favors the attachment and proliferation of human fetal osteoblast (hFOB) osteoprogenitor cells. When soaked in simulated body fluid, enhanced *in vitro* biomineralization occurs on the hybrid membranes. This hybrid membrane holds great promise in biomedical applications such as patches and strips for spine fusion, bone repair, and restoration of tooth enamel.

1. Introduction

Synthetic calcium phosphates (CaPs) are biocompatible, bioactive, and osteoconductive bioceramics that form direct bonds with adjacent hard tissues such as bones and teeth.^[1–4] A variety of CaP phases have been synthesized, including dicalcium phosphate dihydrate (DCPD or brushite), α - and β -tricalcium

phosphates (TCP), octacalcium phosphate (OCP), and hydroxyapatite (HAp).^[1,2] Some of these compounds are Food and Drug Administration (FDA) approved for clinical use and can serve either as bone augmentation cement or as implant coating. In the past several decades, they have been abundantly used in orthopedic and dental applications.^[2] Despite their advantages, CaPs have poor mechanical properties and flexibility. Their inherent rigidity and brittleness make them infeasible for load-bearing applications.^[2,3] Except their use in nonload-bearing implants such as bone void fillers, generally, there are two ways to promote their utilization in load-bearing areas. On the one hand, HAp can serve as a coating on metallic implants to improve their affinity to bone. On the other hand,

HAp could be combined with other mechanically stiffed materials to improve the mechanical performance, including polymers such as collagen, polyvinyl alcohol, chitosan and polyethylene glycol, as well as ceramic microfillers such as alumina and zirconia.^[5] In recent years, due to their good biocompatibility, high mechanical strength, and large specific surface area,^[6] carbon materials could act as an ideal and promising reinforcing agents for CaPs in bone tissue engineering, such as 1D carbon nanotubes (CNTs)^[3,7–10] and 2D graphene (or graphene oxide, GO) nanoflakes, and nanosheets.^[11–13] In recent years, combining HAp with graphene or graphene derivatives have attracted considerable attention. For example, novel tri-component scaffolds consisting of GO, HAp, and polymer have been fabricated by solution mixing and freeze drying method.^[11–13] The mechanical strength is enhanced and the bioactivity of HAp is maintained for osteogenic differentiation and bone regeneration. HAp/GO has also been studied as composite coatings on metal implants by biomineralization,^[14] electrophoretic deposition,^[15–17] vacuum cold spray,^[18] and electrodeposition.^[19] In other cases, HAp was deposited on graphene sheets,^[20] GO sheets,^[21] or functionalized graphene nanosheets.^[22–24] Usually, the nanocomposites are synthesized as nanoparticles in solutions and should be separated by centrifugation. It is also difficult to control the microstructure of HAp crystals.^[25,26]

Some localized diseased or injured areas are in specific configurations, such as damaged articular cartilage and the scratched surface of a dental crown. Thus, flexible membranes

R. J. Zhang, Prof. H. W. Zhu
State Key Laboratory of New Ceramics
and Fine Processing
School of Materials Science and Engineering
Tsinghua University
Beijing 100084, P. R. China
E-mail: hongweizhu@tsinghua.edu.cn

N. Metoki, Prof. N. Eliaz
Biomaterials and Corrosion Lab
Department of Materials Science and Engineering
Tel-Aviv University
Ramat Aviv 6997801, Israel
E-mail: neliaz@tau.ac.il

Dr. O. Sharabani-Yosef
Department of Biomedical Engineering
Tel Aviv University
Ramat Aviv 6997801, Israel

Prof. H. W. Zhu
Center for Nano and Micro Mechanics
Tsinghua University
Beijing 100084, P. R. China



DOI: 10.1002/adfm.201602088

are required to fit the configuration of the target sites. A few flexible films based on CaPs have been investigated.^[27–30] For pure HAp films, the mechanical properties of their free-standing HAp sheets are relatively poor and the process is time-consuming. For example, Nishikawa et al. prepared flexible HAp sheet by pulsed laser deposition with subsequent dissolution of the soluble substrate.^[27] Later, this team attached the sheets directly to the tooth surface for enamel regeneration and conservation.^[28,29] For flexible membranes containing HAp and polymers, on one hand, in most of the previous methods, organic solvents were used,^[30] which might be harmful to the cells and host tissues. On the other hand, the ceramics are easy to be covered with polymers, restricting their exposure to the seeded osteogenic cells and decreasing the bioactivity of the composite scaffolds.^[31] Therefore, the development of physically flexible, mechanically robust, and biocompatible membranes is an important research topic.

Many techniques have been studied for the preparation of CaP coatings on target substrates, including sol–gel synthesis, biomimetic process, pulsed laser deposition, plasma spray, and hydrothermal processing.^[2] However, there are several disadvantages to these methods, such as long preparation term, high temperature, and relatively poor crystallinity. As a simple, low-cost and low-temperature process, electrodeposition has been used to form uniform coatings with low internal stresses and easy control of the deposition rate and structure, even on substrates with complex shapes.^[32–43]

In this work, we prepared flexible, freestanding mesoporous graphene/single-walled carbon nanotubes (MG/SWCNT) hybrid membranes. Some of the membranes were either nitrogen doped or oxygen plasma etched. Subsequently, HAp coating was electrodeposited by a simple, low-cost process.

Well-aligned prismatic hexagonal bars of HAp crystals that resemble the biological mineral were thus formed. The size and chemical composition of the HAp crystals were adjusted through pretreatment of the carbon substrate. *In vitro* cell culture and biomineralization tests show that the HAp-coated hybrid membranes are bioactive and biocompatible for tissue regeneration applications. To the best of our knowledge, this is the first report of a freestanding, flexible HAp membrane that combines a carbon membrane and electrodeposition process. The formation of a bioinspired HAp coating further adds to the clinical significance of this work.

2. Results and Discussion

2.1. Electrodeposition of CaP Coating on Flexible Carbon Substrates

Figure 1a shows the schematic diagram for the electrodeposition of hybrid membranes. Three kinds of flexible carbon-based membranes were used as the working electrodes, including MG/SWCNT hybrid membrane, nitrogen-doped MG/SWCNT (N-MG/SWCNT) membrane and oxygen plasma treated MG/SWCNT (O-MG/SWCNT) membrane. The MG/SWCNT hybrid substrate was prepared using a soft-templated strategy with subsequent vacuum filtration method, with details given in the experimental section. Nitrogen doping of the membranes was conducted in urea solution by hydrothermal method. Oxygen plasma was performed to introduce hydrophilic oxygen-containing functional groups on the surface of MG/SWCNT. After the deposition process, the products are denoted CaP@MG/SWCNT, CaP@N-MG/SWCNT, and CaP@O-MG/SWCNT,

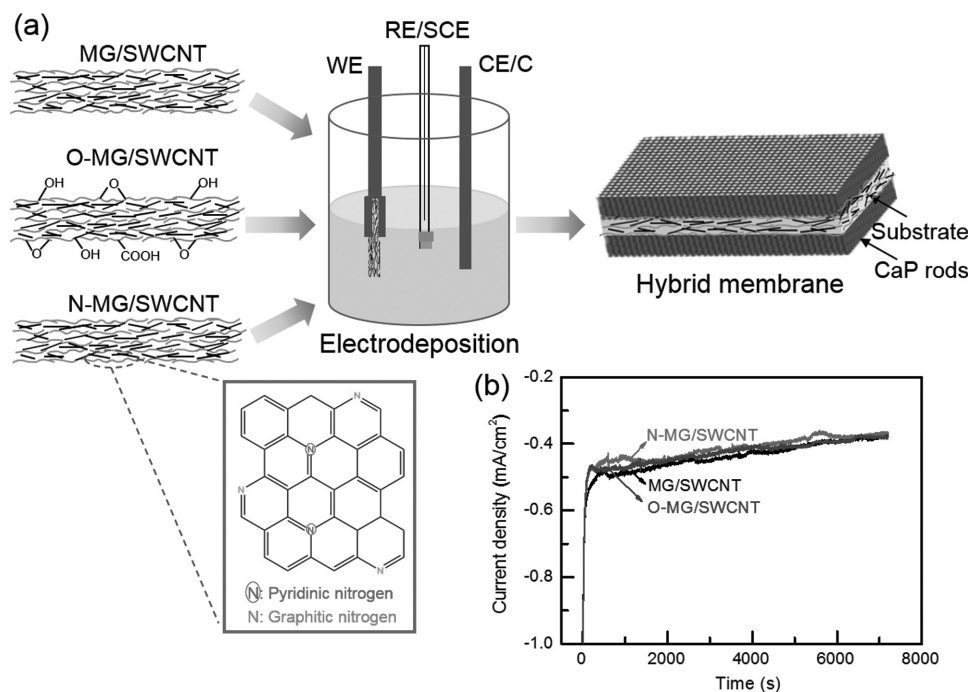


Figure 1. a) Schematic diagram for the synthesis of CaP coating on flexible carbon-based membranes by electrodeposition. b) Current transients of three types of membranes during the deposition process.

respectively. The typical deposition current density curves at constant potential of -1.4 V are shown in Figure 1b. It can be seen that in all three cases the initial cathodic charging current decayed rapidly and attained a steady-state current within a few minutes. Moreover, during deposition the current density dropped slightly due to the increasing electrical resistance of the hybrid membranes. Yet, no significant difference was observed between the current transients of the three membranes. This suggests that the kinetics of deposition was not affected by the doping of the membrane and that the deposition mechanism and the electrochemical reactions involved may be similar.

2.2. Characterization of the CaP Coating on the Flexible Substrates

X-ray photoelectron spectroscopy (XPS) spectra survey of the substrates was conducted, showing effective nitrogen doping and oxygen plasma etching (Figure S1, Supporting Information). As expected, there was a weak N1s peak appearing at ≈ 400 eV in the XPS survey spectrum of N-MG/SWCNT, indicating the effective nitrogen doping with a nitrogen atomic content of about 2.1%. After oxidation, an apparent increase

of the oxygen content was observed, with the C/O atomic ratio decreased from 13.7 for MG/SWCNT to 2.2 for O-MG/SWCNT. High-resolution spectra revealed that oxygen plasma treatment provided carboxyl/carboxylate functional groups on the surface of the substrates (Figure S2a, Supporting Information). These were shown to be crucial for the nucleation and formation of CaP coatings.^[9,28] High-resolution spectra of N1s was fitted by three peaks, corresponding to pyridinic nitrogen at 398.3 eV, pyrrolic nitrogen at 399.7 eV, and graphitic nitrogen at 401.8 eV, respectively (Figure S2c, Supporting Information). Figure S2d–f in the Supporting Information shows scanning electron microscopy (SEM) images of substrates, and Figure S2g–i in the Supporting Information shows the magnification of d–f, respectively. Graphene and SWCNTs coexist in the MG/SWCNT membrane, demonstrating uniform hybrid structures. There was no significant difference in microstructure between MG/SWCNT and N-MG/SWCNT. However, defects and etch pits on the surface of O-MG/SWCNT membrane were observed, showing the effective exfoliation and oxidation of the material during the oxygen plasma etching process (Figure S2f, Supporting Information).

The surface coverage, surface morphology, and microstructure of the CaP coatings are demonstrated in Figure 2. SEM

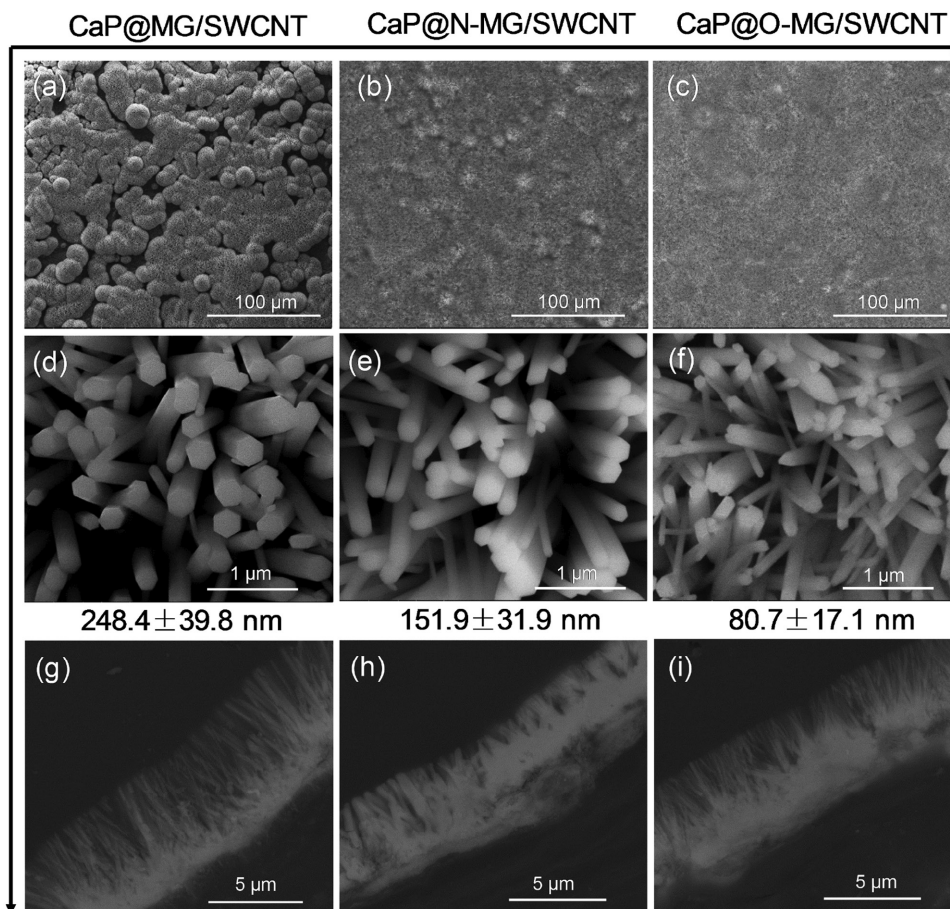


Figure 2. a–c) SEM top-view images of CaP@MG/SWCNT, CaP@N-MG/SWCNT, and CaP@O-MG/SWCNT. CaP@O-MG/SWCNT exhibits the best uniformity. d–f) Higher magnification images of (a–c), respectively. The coating consists of hexagonal prism-shaped CaP crystals. The diameters of the rods are marked under the images. g–i) Corresponding cross-section SEM images. A well-aligned structure is evident.

images of the coatings show well-organized needle-shape CaP crystals, which are actually prismatic hexagonal bars (Figure 2d–f) similar to those observed before on titanium substrates.^[32–34] These needles are arranged in aggregates with a distinct preferred orientation. Using MG/SWCNT membranes as substrates, the CaP coating was not very uniform, showing some crystal bundles (Figure 2a). The uniformity of coatings on pretreated substrates was distinct from that on nontreated substrates. The coating on the pretreated substrates was more uniform, with higher packing density of crystals (Figure 2b,c).

The difference in uniformity could be explained by the functional groups on the surface, the hydrophilicity of substrates, and their intrinsic morphology. We speculate that the doped and etched surfaces created more nucleation sites for CaP on the surface of the membrane. It is known that during the biomineralization process *in vivo*, HAp is associated with the organization of collagen fibers. Interfacial interactions exist between HAp and the functional groups of the side chains of the collagen molecules, where hydroxyl and carboxyl groups are abundant.^[44–46] Furthermore, the study of CaP biomimetic nucleation on self-assembled monolayers has revealed that not only negative end groups containing oxygen would assist nucleation, but also positively charged amine groups.^[44,45] Thus, the added functional groups on top of the N-doped and oxygen plasma treated membranes and the defects on the surface (Figure S2, Supporting Information) increased the number of nucleation sites for electrodeposited CaP, thus improving the uniformity of the coatings farther.

The formation of crystals with a prismatic hexagonal bar shape is interesting from scientific, technological, and clinical standpoints. The outer shape of a crystal, as observed by SEM, is often related to the point group symmetry to which the crystal belongs. Hence, it is likely that each bar in Figure 2d–f is a single crystal of HAp. Single crystals of the biological HAp have hexagonal space group $P6_3/m$. Thus, the microstructure of the electrochemically deposited HAp coating resembles that of bone, which may have a clinical value with respect to osteoconduction and osteointegration. The crystal diameters noted in Figure 2 are similar to values of 300 nm^[32,33] and 100 nm^[34] reported before by Eliaz et al. for electrodeposited HAp on titanium pretreated both mechanically (e.g., grit blasted) and chemically (e.g., soaked in NaOH). The mean diameter of the bars changed in the order CaP@MG/SWCNT > CaP@N-MG/SWCNT > CaP@O-MG/SWCNT. This difference could be explained by increased density of preferred nucleation sites following nitrogen doping, and even more following oxygen plasma etching. The smallest crystals are more similar in dimension to the natural apatite, which has been reported to be in the range of several nm to more than 100 nm.^[40,47,48] The size and shape of bone apatite crystals actually change with species and age.^[40,48] The similarity in size and shape of the CaP crystals in the CaP@O-MG/SWCNT and the biological apatite could be beneficial for *in vivo* applications. Moreover, smaller crystal size has been reported to be more beneficial thanks to higher surface area that facilitates additional adsorption of ions and molecules, thus permitting faster regeneration of tissues.^[4]

The crystal shape in electrodeposits is sensitive to many variables, including substrate material, surface pre-treatments, bath chemistry, pH, temperature, stirring, etc. From scientific

standpoint it is thus interesting that similar crystals grow on Ti-6Al-4V alloy and CP-Ti that were mechanically and chemically pretreated and on MG/SWCNT that was not pretreated at all. It also indicates that soaking in NaOH was not responsible for the formation of hexagonal crystals in the previous work of Eliaz et al. It seems that the pH of the solution is most influential in this regard. From technological standpoint, the ability to form good CaP coatings while eliminating the pretreatment stages is beneficial from time and cost perspectives.

Based on cross-sections of the samples (Figure 2g–i), the thickness of all coatings is $\approx 5.5 \pm 0.5 \mu\text{m}$, thus the deposition rate is about $2.8 \mu\text{m h}^{-1}$. This deposition rate may satisfy industrial specifications. In addition, it is evident that the coating is comprised of two layers: (i) a uniform dense layer adjacent to the substrate; and (ii) a thicker layer with columnar crystals. This observation is similar to that reported and discussed by Eliaz and co-workers.^[40,42]

In order to further examine the underlying reasons of the different uniformity of the coatings, contact angle measurements of sessile water drop were performed. The test was done on the three different substrates, (Figure S3a–c, Supporting Information). It was discovered that the MG/SWCNT membrane was the most hydrophobic among the three membranes, with contact angles of $94.3 \pm 3.1^\circ$, followed by N-MG/SWCNT with $76.6 \pm 3.2^\circ$. O-MG/SWCNT was externally hydrophilic ($\theta < 24^\circ$, no measurements were made). These results are in good agreement with the XPS measurements that reveal the hydrophilic functional groups on the surface. The coating is apparently more uniform as the hydrophilicity of the substrate increases (Figure 2a–c). After electrochemical deposition, all CaP coatings on the different hybrid membranes are superhydrophilic (Figure S3d–f, Supporting Information).

To further characterize the structure and chemical composition of the coating, energy-dispersive X-ray spectroscopy (EDS), XPS, and X-ray diffraction (XRD) measurements were conducted. Table 1 shows the Ca/P ratio based on EDS analysis. The values are in the range of 1.51 and 1.57, indicating potentially the same phase content. Yet, it should be noted that EDS analysis has been reported to be unreliable for electrodeposited CaP compared with advanced XPS analyses.^[32–34] XPS survey spectra (not shown here) acquired from all samples revealed Ca, P, and O from the CaP coating, as well as C from carbonate contamination on the surface. The atomic concentration of the elements obtained from high-resolution XPS measurements, together with the Ca/P and O/Ca atomic ratios, are shown in Table 2. For comparison, the theoretical Ca/P ratios are 1.00, 1.33, 1.50, 1.50, and 1.67 for DCPD, OCP, amorphous calcium phosphate (ACP), TCP and HAp, respectively, and the theoretical O/Ca ratios for these phases are 6.00, 3.125, 3.00, 2.67, and 2.60, respectively.^[37,49] In order to identify the phases unambiguously, the oxygen loss spectrum was analyzed. The values of $O(1s)_{II}/O(1s)$ are also provided in Table 2. In comparison,

Table 1. The calcium-to-phosphorous atomic ratio based on EDS data.

| Coating | CaP@MG/SWCNT | CaP@N-MG/SWCNT | CaP@O-MG/SWCNT |
|---------|-----------------|-----------------|-----------------|
| Ca/P | 1.57 ± 0.02 | 1.55 ± 0.00 | 1.51 ± 0.08 |

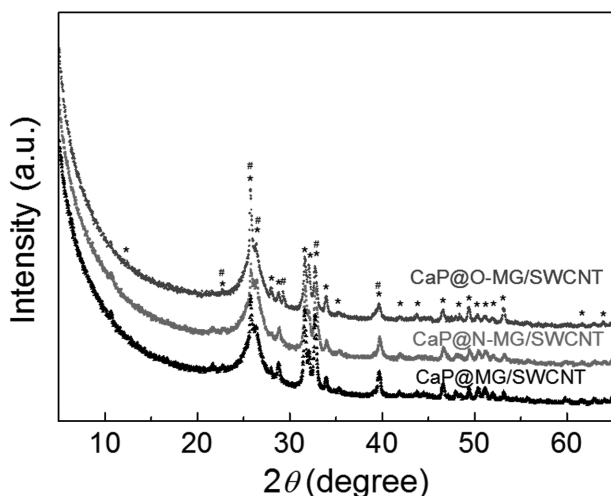
Table 2. Chemical composition (at%) determined by XPS.

| Element | CaP@MG/SWCNT | CaP@N-MG/SWCNT | CaP@O-MG/SWCNT |
|-----------------------------|--------------|----------------|----------------|
| C | 13.36 | 14.88 | 11.85 |
| O | 56.53 | 54.77 | 56.10 |
| Ca | 16.39 | 18.31 | 18.10 |
| P | 13.71 | 12.05 | 13.95 |
| Ca/P | 1.20 | 1.52 | 1.30 |
| O/Ca | 3.45 | 2.99 | 3.10 |
| O(1s) _{III} /O(1s) | 0.057 | 0.068 | 0.062 |

Lu et al.^[49] and Metoki et al.^[36] measured mean O(1s)_{III}/O(1s) ratios of 0.072, 0.065, 0.053, 0.037, 0.020, and 0.008 for powders of TCP, HAp, OCP, DCPA, DCPD, and monobasic calcium phosphate monohydrate, respectively.

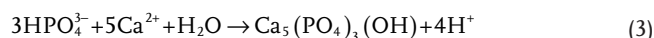
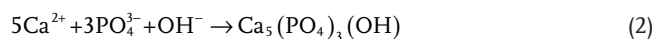
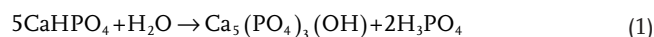
The XPS data could be matched to the theoretical values of the OCP phase alone in the case of MG/SWCNT membrane. However, for the coating on N-MG/SWCNT membrane, a possible match could be to 92% HAp + 8% DCPD, while for that on O-MG/SWCNT several options were suggested: 51% OCP + 49% TCP, 78% OCP + 22% DCPD, and 84% TCP + 16% DCPD.

XRD measurements were conducted to better determine the phase content of different coatings (**Figure 3**). All reflections of CaP@MG/SWCNT and CaP@N-MG/SWCNT are assigned to HAp (JCPDS 04-015-6216), with preferred (002) orientation. CaP@O-MG/SWCNT gave rise to a secondary organic phase of aminoguanidium 5-nitrotetrazole (CN₄H₇)(CN₅O₂), JCPDS 04-015-5798. The organic phase, the origin of which could be either the substrate or the oxygen plasma, constitutes ≈10% of the coating, based on XRD analysis. Given the complete indexing of reflections by XRD, the similar hexagonal shape of crystals as evident by SEM, and a previously reported contradiction between XRD and XPS results,^[34] we believe that all three coating types consist of a single HAp phase. Analysis of XRD data also yielded crystallite sizes of 41.1, 37.9, and 26.2 nm for

**Figure 3.** XRD patterns from CaP@MG/SWCNT, CaP@N-MG/SWCNT, and CaP@O-MG/SWCNT. * HAp (JCPDS 04-015-6216), # (CN₄H₇)(CN₅O₂) (JCPDS 04-015-5798).

CaP@MG/SWCNT, CaP@N-MG/SWCNT, and CaP@O-MG/SWCNT, respectively. These results are in line with the measurements of crystal sizes on SEM images (**Figure 2**). Again, the density of nucleation sites at the surface of the O-MG/SWCNT is evidently the highest.

Following previous publications^[32–42] and the analysis of phase content by XRD, a proposed mechanism for deposition can be suggested. We believe that the electrodeposition of HAp from solution is not a direct, conventional one.^[32–42] The majority of current is spent on the reduction of water and the elevation of pH in the vicinity of the electrode.^[40] Following the pH elevation, the phosphoric acid in solution deprotonates, and is then free to form chemical reactions. The proposed chemical reactions for HAp are



In order to monitor the evolution of HAp crystal growth on MG/SWCNT, SEM images were taken after 10, 30, and 60 min of deposition (**Figure S4a–c**, Supporting Information). The crystal shape after 10 min is significantly different from that after 30 and 60 min, and appears to be a stack of nano-sized crystallites (**Figure S4a**, Supporting Information). This nanostructure and the time frame correlate well with the uniform dense layer adjacent to the substrate in **Figure 1g**. Eliaz and co-workers have observed a transition from instantaneous nucleation and 2D growth to progressive nucleation and 3D growth after ≈12 min electrodeposition of CaP on titanium.^[37,40,42] It was suggested that a layer of OCP first formed and served as a precursor for HAp. It was also claimed that a local pH elevation, in the vicinity of the cathode, is a driving force for this transition. From **Figure S4b,c** in the Supporting Information it is evident that the diameter of the rods did not change between 30 and 60 min, only the thickness of the coating increased, which is typical of a columnar growth.

2.3. Cell Adhesion and Proliferation Test

Cell adhesion properties are of great importance for the bonding of implants to their surrounding tissues.^[50] Moreover, they give insight to the biocompatibility of the patches. hFOB osteoprogenitor human cells were cultured on the CaP@MG/SWCNT, CaP@N-MG/SWCNT, and CaP@O-MG/SWCNT membranes, as well as on reference membranes, for time periods of 1 and 3 d. SEM images of the 1 d culturing on the coated samples are shown in **Figure 4**. The cells are distributed on the coating (**Figure 4a–c**), and appear to be flattened on top of it (**Figure 4d–f**). At high magnification (**Figure 4g–i**), the cytoplasmic membrane seems to be very thin (semitransparent) and stretched over the HAp needles. Filopodia which penetrate into pores and grasp the CaP bars assist the cell in its morphological change. This behavior is known as “gap guidance”. No rounded cells are evident. The above observations are indicative of enhanced focal adhesion (or cell attachment).^[33]

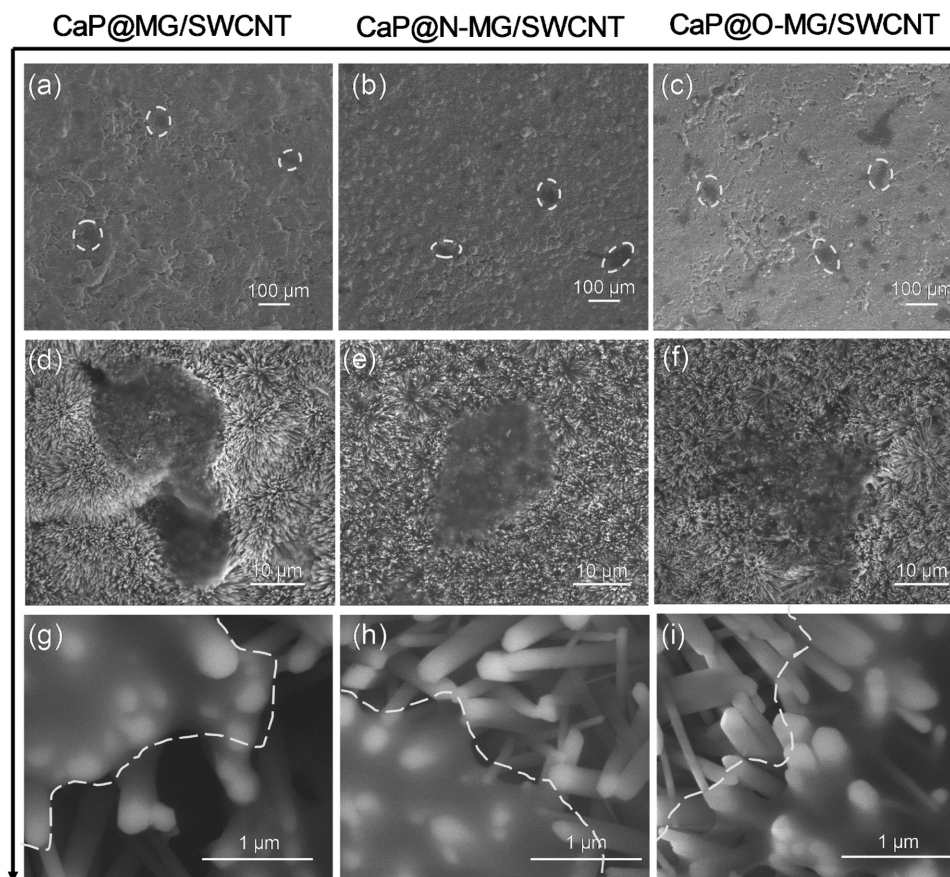


Figure 4. SEM images of hFOB cells cultured for 1 d on a,d,g) CaP@MG/SWCNT, b,e,h) CaP@N-MG/SWCNT, and c,f,i) CaP@O-MG/SWCNT. Images at low magnification indicate the cell density while those at high magnification reveal the cell morphology and attachment to the coating. The cells adhere well to the surface, proving that it is not cytotoxic. Images (g–i) show the thin cytoplasmic membrane with filopodia at the edges of the cells.

SEM images after 3 d culturing are shown in Figure S5 in the Supporting Information. Many cells are attached to the surface. Figure S5a–f in the Supporting Information shows the stretched and elongated cells, with visible filopodia and lamellipodia (Figure S5g–i, Supporting Information). The filopodia penetrate into pores and grasp the needles to assist in stretching the cells. From these images it is evident that the hybrid membranes are not cytotoxic for the cells, and that the coating is highly bioactive. Low contrast between the seeded cells and the substrates of the uncoated samples prevented us from obtaining informative SEM images. A complementary light microscope characterization is therefore used.

Figure 5 reveals the fluorescence micrographs of hFOB cells cultured for 3 d on uncoated (Figure 5a–c) and coated membranes (Figure 5d–f). The cells were counted on at least three different locations on each membrane, and each membrane had two duplicates in the experiment. Cell count histograms following 3 d culturing are shown in Figure 5g. Analysis of variance (ANOVA) analysis on the uncoated membranes revealed that the type of membrane did not have an effect on the number of cells counted ($p = 0.751$). This indicated that the doping of the membranes did not affect the adhesion of cells, or the cytotoxicity of the substrate. From Figure 5 it is also evident that the density of cells increased on the HAp-coated membranes compared to their corresponding uncoated membranes. Thus, the

HAp coating establishes a bioactive surface, as expected. This is due to its chemistry, structure, and the formation of a superhydrophilic surface, to which osteoblasts have a strong preference in their adhesion and proliferation.^[33]

The number of cells attached to the coated substrates was also evaluated by ANOVA analysis and a post-hoc Tukey test was also conducted for multiple comparisons. This was done using the Bonferroni correction ($\alpha^* = \alpha/n$, where $\alpha = 0.05$ is the level of significance and $n = 3$ is the number of groups). The coated substrates indicated an overall significant difference among the groups ($p = 0.000$). A differentiation among the subgroups was done by post-hoc Tukey test. It was thus found that CaP@MG/SWCNT versus CaP@N-MG/SWCNT, CaP@MG/SWCNT versus CaP@O-MG/SWCNT, and CaP@O-MG/SWCNT versus CaP@N-MG/SWCNT were all significantly different ($p = 0.000$, 0.004 , and 0.004 , respectively, $\alpha^* = 0.017$). From Figure 5 it is evident that more bone-forming cells were attached to CaP coatings on pretreated membranes, with the beneficial effect of nitrogen doping being the highest. This could be attributed to the high hydrophilicity of the coating as well as to abundant nitrogen groups on the surface of the membrane beneath it. Nitrogen and carbon are substantial building block in all amino acids.^[51] Moreover, the relationship between amino acids and cell proliferation has long been studied.^[52] We speculate that the outer surface of the CaP@N-MG/SWCNT

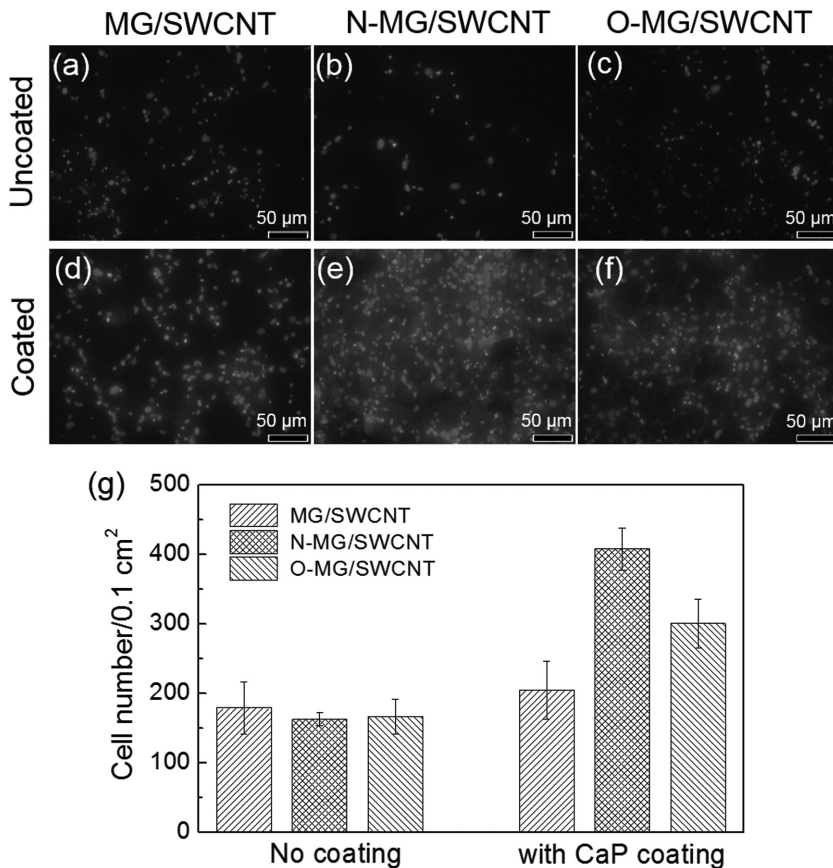


Figure 5. Fluorescence micrographs of hFOB cells cultured for 3 d on the three types of membranes a–c) before and d–f) after CaP coating. g) Corresponding cell count histograms.

is richer in nitrogen-containing groups, which are exposed to the growth medium. Another explanation could be that the secondary organic phase of aminoguanidium 5-nitrotetrazole

mud-cracks is evident. This observation indicates the formation of a thick biomimetic CaP layer on top of the synthetic HAp coating. EDS analysis (not shown here) showed high

detected by XRD only in the case of CaP@O-MG/SWCNT (Figure 3) lowers cell attachment compared to CaP@N-MG/SWCNT, although based on SEM (Figure 2) the crystal size of the former is smaller and closer to that of biological apatite.

When comparing each type of uncoated membrane to its corresponding coated membrane it is concluded that the difference in cell density is not significant ($p = 0.301$) in the case of MG/SWCNT, but is significant in the case of O-MG/SWCNT and N-MG/SWCNT ($p = 0.000$ for both). This may be the result of the CaP@MG/SWCNT coating being nonuniform, not fully covering the surface of the substrate, and with larger HAp needles (i.e., less needles per unit area).

2.4. In Vitro Biomineralization

Figure 6a–f show the HAp-coated membranes after biomineralization assay. The samples were immersed in five-time concentrated simulated body fluid (SBF) solution for 7 d. Clearly, the coatings show high bioactivity. Nevertheless, the biomineralized deposits are nonuniform and exhibit globular crystal agglomerates on the surface. Their surface morphology is also vastly different from that in Figure 2. The hexagonal crystals are not evident after biomineralization; instead, a layer with

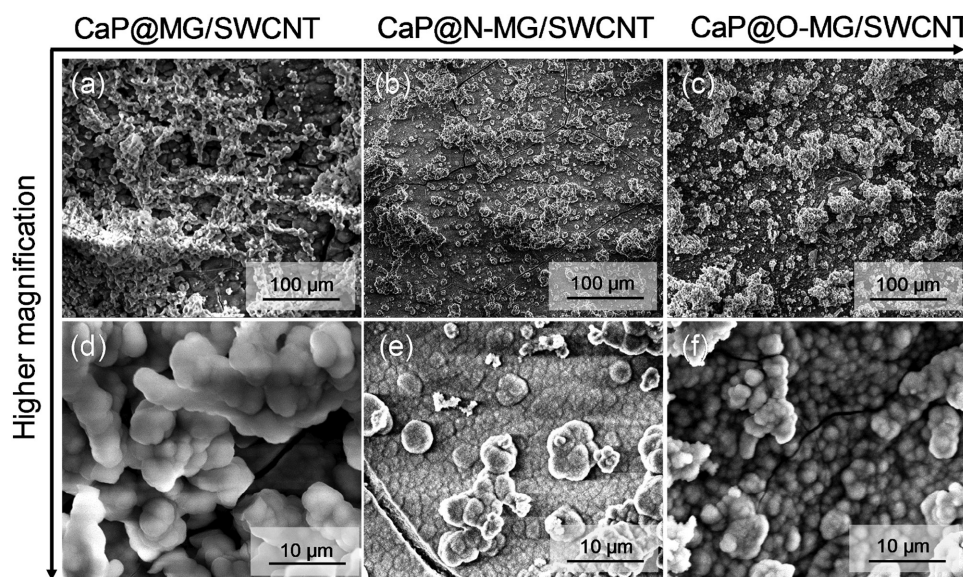


Figure 6. SEM images of apatite formed on a,d) CaP@MG/SWCNT, b,e) CaP@N-MG/SWCNT, and c,f) CaP@O-MG/SWCNT after soaking in 5× SBF for 7 d.

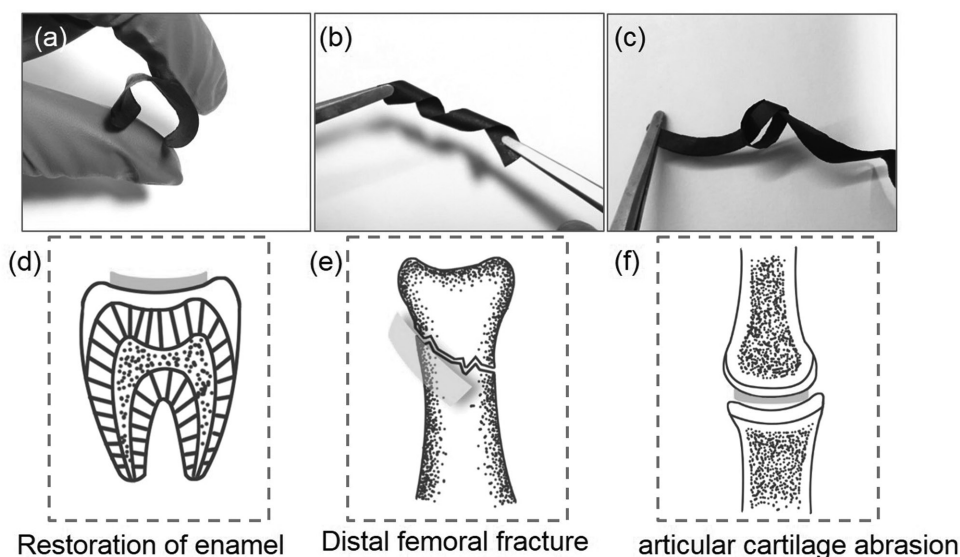


Figure 7. Excellent flexibility of the hybrid membrane under a) bending, b) twisting, and c) knotting. Schematics of potential applications of the HAp@N-MG/CNT hybrid membranes, including d) tooth enamel restoration, e) patches or strips in repairing of distal femora, and f) articular cartilage for bone regeneration.

signals of calcium and phosphorous, in addition to chlorine. In contrast, the uncoated membranes show only negligible amount of CaP deposit at few locations following biomineralization assay (Figure S6a–c, Supporting Information). The shape of the biomineralized deposit on uncoated membranes is significantly different than that of HAp-coated membranes (Figure S6d–f, Supporting Information). It may thus be concluded that the HAp-coated membranes have positive effect on biomineralization *in vitro*.

2.5. Flexibility and Potential Applications in Regenerative Medicine

In clinical applications, some bone implants require surface modification or reinforcement. The hybrid membranes prepared in this work are anticipated to be used as patches in bone and tooth repair. For this purpose, additional adhesion tests were performed on the coating. A scotch tape adhesion test revealed that the adhesion of the coating to the membrane is stronger than the membranes cohesion, thus confirming a strong bond between the two. The physical flexibility of the membranes, as demonstrated in Figure 7a–c, is useful for the tight attachment to curved surfaces. From the stress–strain curves (Figure S7, Supporting Information), it can be observed that MG/SWCNT and N-MG/SWCNT show similar mechanical properties, with a fracture strain at $\approx 13\%$. Due to the plasma etching, O-MG/SWCNT shows lower tensile strength. As to the materials obtained after electrodeposition process, because of the intrinsic rigidity and brittleness of CaP coatings, the tensile strength decreases and the Young's modulus increases. The stress–strain curves as well as the flexibility of the materials demonstrate that they are robust enough for clinical utilization.^[53,54] In such cases, they could deliver CaPs directly to diseased areas and assist in reconstruction of the bone by

attracting osteoblasts to the damaged area. The membranes are extremely thin ($14\ \mu\text{m}$) and flexible, and therefore enable to coat irregular surfaces easily. Specifically, they have broad potential applications in fields such as tooth enamel erosion (Figure 7d), distal femoral fractures (Figure 7e), and articular cartilage abrasions (Figure 7f).

3. Conclusion

In conclusion, we have synthesized well-aligned biomimetic hexagonal needles of HAp on flexible, freestanding MG/SWCNT hybrid membranes by a simple, low-cost, and environment friendly electrochemical process. Nitrogen doping and oxygen plasma etching of the MG/SWCNT membranes increased the density of nucleation sites and yielded more uniform coatings with smaller HAp needles. The coated membranes showed excellent biocompatibility and bioactivity *in vitro* based on proliferation test of hFOB osteoprogenitor human cells. They also showed significantly better biomineralization *in vitro*. Nitrogen-doped hybrid membranes gave the best results. The hybrid membranes hold great promise in biomedical applications such as bone repair and restoration of tooth enamel.

4. Experimental Section

Preparation of Porous MG/SWCNT Membranes: MG/SWCNT membranes were prepared using F127 micelles as soft templates, as the authors prepared before.^[55] Briefly, GO suspension was prepared by a modified Hummers method. First, $15\ \mu\text{L}$ hydrazine was added to $7.5\ \text{mL}$ GO aqueous suspension ($2\ \text{g L}^{-1}$) at $90\ ^\circ\text{C}$ for 45 min under vigorous stirring to prepare partially-reduced GO solution. Then, $3\ \text{mL}$ F127 solution (10 wt%) was added and stirred for 2 h. After this, $2\ \text{mL}$ HCl (37 wt%) was added, and the solution was stirred for another 2 h. Subsequently, $15\ \text{mL}$ SWCNT aqueous dispersion ($1\ \text{g L}^{-1}$) was added

to the solution with vigorously stirring for 12 h. The liquid was divided equally into two parts for vacuum filtration process. The obtained hybrid membranes were dried at 55 °C and then annealed at 350 °C for 2 h and next by 900 °C for 1 h in Ar atmosphere.

Synthesis of N-MG/SWCNT Membrane: 2 g urea was first dissolved in 50 mL distilled water. Then, the obtained MG/SWCNT membrane was transferred into a 50 mL Teflon-lined stainless autoclave with 30 mL urea solution. The autoclave was sealed and hydrothermally treated at 180 °C for 12 h. After cooling at ambient temperature, the membrane was removed from the autoclave and washed with distilled water. The N-doped MG/SWCNT membrane was obtained by subsequent freeze-drying process.

Synthesis of O-MG/SWCNT Membrane: Oxygen plasma etching of the membrane was performed by introducing the preobtained MG/SWCNT into a plasma machine (Electronic Diener FEMTIO) for 8 min. In the process, an oxygen flow rate of 1 mL min⁻¹ was provided.

Electrodeposition of HAp Coating: The electrochemical deposition of HAp on MG/SWCNT membrane was carried out using a standard three-electrode system. The hybrid membrane was used as a working electrode (with an exposed surface area of 20 × 5 mm²). Two graphite rods were used as the counter electrodes, and a saturated calomel electrode (SCE) was used as the reference electrode. The solution was prepared by dissolving 0.61 × 10⁻³ M Ca(NO₃)₂ and 0.36 × 10⁻³ M NH₄H₂PO₄ in distilled water. The pH of the solution was adjusted to 6.0 by adding drops of 5 M NaOH solution, and measured by InoLab pH/Oxi Level 3 meter. Potentiostatic deposition was done using an EG&G/PAR 263A potentiostat, operating at -1.4 V versus SCE for 2 h, with the solution being stirred at 200 rpm during deposition. The experiment was carried out at 90 °C. The cell temperature was kept constant by internal and external circulation bath (MRC, WBH-060). After electrodeposition, the membrane was rinsed in distilled water and dried at ambient temperature.

HAp and MG/SWCNT Characterization: The structure of the coating was analyzed by XRD using a Scintag powder diffractometer within the range of 2θ = 0°–100° at a scan rate of 0.05°·s⁻¹. The surface morphology was revealed in an environmental scanning electron microscope (ESEM, Quanta 200 FEG, FEI). The Ca/P atomic ratio of the HAp coating was estimated using EDS. Contact angle measurements were conducted using Ramé–Hart model 100 contact angle goniometer. The values reported here are the averages of three measurements per sample.

Proliferation Test: Proliferation test was done using hFOB Osteoblast Human (ATCC, CRL-11372). Cells were grown and cultured on Petri plates inside an incubator that was set to 37 °C and 5% CO₂. A culturing medium containing 10% fetal bovine serum, 90% Ham's F 12 Dulbecco's Modified Eagle, 0.6% G-418 disulfate salt solution and 1.25% L-Glutamine was used (all constituents of the growth medium were purchased from Biological Industries, Israel). The cells were cultured until reaching >85% confluence, which normally occurred 3–4 d after seeding. When approaching confluency, the cells were trypsinized from the Petri dishes. The cells were then collected, centrifuged, and counted. 1.4 × 10⁵ cells were then seeded on 1.5 mm diameter plates containing the coated and uncoated membranes. 2 mL of growth medium was added to the plates and left to grow for either 1 or 3 d. The growth medium was removed, and the specimens were washed twice with phosphate-buffered saline. The cells were fixed using 100 μL of ethanol absolute. Next, the cells were fluorescence-stained using DAPI staining, and examined by fluorescence microscope (Olympus IX71, Tokyo, Japan). Statistical analysis of the cell count on fluorescence microscope images was performed using Statistical Package for the Social Sciences (SPSS) statistical analysis program. ANOVA was used for multiple comparisons, with a post-hoc Tukey test using a Bonferroni correction.

Biom mineralization: Biom mineralization was tested in ×5 SBF solution that was prepared as described by Kokubo and Takadama.^[56] The samples were placed in 15 mL solution of ×5 SBF at pH 7.40 for 7 d. Every 2 d the solution was replaced by fresh solution, and the samples were kept in an incubator operating at 37 °C. After 7 d, the samples were washed, dried, and examined by ESEM.

Supporting Information

Supporting Information is available from the Wiley Online Library or from the author.

Acknowledgements

R.J.Z. and N.M. contributed equally to this work. R.J.Z. prepared the flexible carbon-based membranes and characterized them by XPS at Tsinghua University. All other experiments were carried out at Tel-Aviv University, where R.J.Z. was a visiting scholar. The authors thank Yuri Rosenberg and Larisa Burstein from the Wolfson Applied Materials Research Centre at Tel-Aviv University for collection of XRD and XPS data, respectively. The authors thank also Mario Levishtein for his technical assistance. R.Z. thanks the Innovative Talents Program initiated by the XIN Center (co-founded by Tsinghua University and Tel-Aviv University) and China Ministry of Education for their financial support. H.Z. thanks the National Science Foundation of China (51372133).

Received: April 25, 2016

Revised: September 11, 2016

Published online: October 13, 2016

- [1] S. V. Dorozhkin, M. Epple, *Angew. Chem. Int. Ed.* **2002**, *41*, 3130.
- [2] M. Valletregi, *Prog. Solid State Chem.* **2004**, *32*, 1.
- [3] A. A. White, S. M. Best, I. A. Kinloch, *Int. J. Appl. Ceram. Technol.* **2007**, *4*, 1.
- [4] L. C. Palmer, C. J. Newcomb, S. R. Kaltz, E. D. Spoerke, S. I. Stupp, *Chem. Rev.* **2008**, *108*, 4754.
- [5] W. Suchanek, M. Yoshimura, *J. Mater. Res.* **1998**, *13*, 94.
- [6] S. H. Ku, M. Lee, C. B. Park, *Adv. Healthcare Mater.* **2013**, *2*, 244.
- [7] J. Zhu, H. M. Wong, K. W. K. Yeung, S. C. Tjong, *Adv. Eng. Mater.* **2011**, *13*, 336.
- [8] I. A. Siqueira, C. A. Oliveira, H. Zanin, M. A. Grinet, A. E. Granato, M. A. Porcionatto, F. R. Marciano, A. O. Lobo, *J. Mater. Sci.: Mater. Med.* **2015**, *26*, 113.
- [9] H. Zanin, C. M. Rosa, N. Eliaz, P. W. May, F. R. Marciano, A. O. Lobo, *Nanoscale* **2015**, *7*, 10218.
- [10] P. Khalid, M. A. Hussain, P. D. Rekha, A. B. Arun, *Human Exp. Toxicol.* **2015**, *34*, 548.
- [11] M. Nair, D. Nancy, A. G. Krishnan, G. S. Anjusree, S. Vadukumpully, S. V. Nair, *Nanotechnology* **2015**, *26*, 161001.
- [12] R. Rajesh, Y. D. Ravichandran, *RSC Adv.* **2015**, *5*, 41135.
- [13] G. Xiong, H. Luo, G. Zuo, K. Ren, Y. Wan, *Mater. Character.* **2015**, *107*, 419.
- [14] F. Gao, C. Xu, H. Hub, Q. Wang, Y. Gao, H. Chen, Q. Guo, D. Chen, D. Eder, *Mater. Lett.* **2015**, *138*, 25.
- [15] M. Li, Q. Liu, Z. Jia, X. Xu, Y. Cheng, Y. Zheng, T. Xi, S. Wei, *Carbon* **2014**, *67*, 185.
- [16] A. Janković, S. Eraković, M. Mitrić, I. Z. Matić, Z. D. Juranić, G. C. P. Tsui, C. Tang, V. Mišković-Stanković, K. Y. Rhee, S. J. Park, *J. Alloys Compd.* **2015**, *624*, 148.
- [17] C. Santos, C. Piedade, P. J. Uggowitzer, M. F. Montemor, M. J. Carmezim, *Appl. Surf. Sci.* **2015**, *345*, 387.
- [18] Y. Liu, J. Huang, H. Li, *J. Therm. Spray Technol.* **2014**, *23*, 1149.
- [19] H. Zanin, E. Saito, F. R. Marciano, H. J. Ceragioli, A. E. C. Granato, M. Porcionatto, A. O. Lobo, *J. Mater. Chem. B* **2013**, *1*, 4947.
- [20] C. Rodríguez-González, H. E. Cid-Luna, P. Salas, V. M. Castaño, *J. Nanomater.* **2014**, 940903.
- [21] J. D. Núñez, A. M. Benito, R. González, J. Aragón, R. Arenal, W. K. Maser, *Carbon* **2014**, *79*, 590.

- [22] Q. Zhang, Y. Liu, Y. Zhang, H. Li, Y. Tan, L. Luo, J. Duan, K. Lia, C. E. Banks, *Analyst* **2015**, *140*, 5235.
- [23] J. Wang, Z. Ouyang, Z. Ren, J. Li, P. Zhang, G. Wei, Z. Su, *Carbon* **2015**, *89*, 20.
- [24] G. M. Neelgund, A. Oki, Z. Luo, *Mater. Res. Bull.* **2013**, *48*, 175.
- [25] X. Xie, K. Hu, D. Fang, L. Shang, S. D. Tran, M. Cerruti, *Nanoscale* **2015**, *7*, 7992.
- [26] Y. Li, C. Liu, H. Zhai, G. Zhu, H. Pan, X. Xuab, R. Tang, *RSC Adv.* **2014**, *4*, 25398.
- [27] H. Nishikawa, R. Hatanaka, M. Kusunoki, T. Hayami, S. Hontsu, *Appl. Phys. Express* **2008**, *1*, 088001.
- [28] S. Hontsu, K. Yoshikawa, N. Kato, Y. Kawakami, T. Hayami, H. Nishikawa, M. Kusunoki, K. Yamamoto, *J. Aust. Ceram. Soc.* **2011**, *47*, 11.
- [29] E. Yamamoto, N. Kato, A. Isai, H. Nishikawa, M. Kusunoki, K. Yoshikawa, S. Hontsu, *Bioceram. Dev. Appl.* **2013**, *S1*, 006.
- [30] D. Depan, T. C. Pesacretab, R. D. K. Misra, *Biomater. Sci.* **2014**, *2*, 264.
- [31] S.-S. Kim, M. S. Park, O. Jeon, C. Y. Choi, B.-S. Kim, *Biomater.* **2006**, *27*, 1399.
- [32] D. Lakstein, W. Kopelovitch, Z. Barkay, M. Bahaa, D. Hendel, N. Eliaz, *Acta Biomater.* **2009**, *5*, 2258.
- [33] N. Eliaz, S. Shmueli, I. Shur, D. Benayahu, D. Aronov, G. Rosenman, *Acta Biomater.* **2009**, *5*, 3178.
- [34] N. Eliaz, O. Ritman-Hertz, D. Aronov, E. Weinberg, Y. Shenhar, G. Rosenman, M. Weinreb, E. Ron, *J. Mater. Sci.: Mater. Med.* **2011**, *22*, 1741.
- [35] N. Eliaz, *Israel J. Chem.* **2008**, *48*, 159.
- [36] N. Metoki, L. Leifenberg-Kuznits, W. Kopelovich, L. Burstein, M. Gozin, N. Eliaz, *Mater. Lett.* **2014**, *119*, 24.
- [37] N. Eliaz, W. Kopelovitch, L. Burstein, E. Kobayashi, T. Hanawa, *J. Biomed. Mater. Res.. Part A* **2009**, *89*, 270.
- [38] N. Eliaz, T. M. Sridhar, U. Kamachi Mudali, B. Raj, *Surf. Eng.* **2005**, *21*, 238.
- [39] H. Wang, N. Eliaz, Z. Xiang, H.-P. Hsu, M. Spector, L. W. Hobbs, *Biomaterials* **2006**, *27*, 4192.
- [40] N. Eliaz, M. Eliyahu, *J. Biomed. Mater. Res. A* **2007**, *80*, 621.
- [41] N. Eliaz, T. M. Sridhar, *Cryst. Growth Des.* **2008**, *8*, 3965.
- [42] H. Wang, N. Eliaz, L. W. Hobbs, *Mater. Lett.* **2011**, *65*, 2455.
- [43] B. León, J. A. Jansen, *Thin Calcium Phosphate Coatings for Medical Implants*, Springer Science, NY, USA **2009**.
- [44] M. Tanahashi, T. Matsuda, *J. Biomed. Mater. Res.* **1997**, *34*, 305.
- [45] P. J. Majewski, G. Allidi, *Mat. Sci. Eng. A* **2006**, *420*, 13.
- [46] D. P. Liu, P. Majewski, B. K. O'Neill, Y. Ngothai, C. B. Colby, *J. Biomed. Mater. Res. Part A* **2006**, *77*, 763.
- [47] Q. Liu, S. Huang, J. P. Matinlinna, Z. Chen, H. Pan, *BioMed Res. Int.* **2013**, *2013*, 929748.
- [48] C. Rey, C. Combes, C. Drouet, M. J. Glimcher, *Osteoporos. Int.* **2009**, *20*, 1013.
- [49] H. B. Lu, C. T. Campbell, D. J. Graham, B. D. Ratner, *Anal. Chem.* **2000**, *72*, 2886.
- [50] M. Uchida, A. Oyane, H. M. Kim, T. Kokubo, A. Ito, *Adv. Mater.* **2004**, *16*, 1071.
- [51] G. Wu, *Amino Acids: Biochemistry and Nutrition*, CRC Press, Taylor and Francis, Boca Raton, FL, USA **2013**.
- [52] B. Szende, *Acta Biomed. Ateneo Parmense* **1993**, *64*, 139.
- [53] H. Chen, M. B. Muller, K. J. Gilmore, G. G. Wallace, D. Li, *Adv. Mater.* **2008**, *20*, 3557.
- [54] J. Shi, X. Li, H. Cheng, Z. Liu, L. Zhao, T. Yang, Z. Dai, Z. Cheng, E. Shi, L. Yang, Z. Zhang, A. Cao, H. Zhu, Y. Fang, *Adv. Funct. Mater.* **2016**, *26*, 2078.
- [55] R. Zhang, X. Li, L. Zhang, S. Lin, H. Zhu, *Adv. Sci.* **2016**, DOI: 10.1002/advs.201600208.
- [56] T. Kokubo, H. Takadama, *Biomaterials* **2006**, *27*, 2907.